Applied Catalysis B: Environmental 178 (2015) 177–185

Contents lists available at ScienceDirect

Applied Catalysis B: Environmental

journal homepage: www.elsevier.com/locate/apcatb

Effect of Au surface plasmon nanoparticles on the selective CO_2 photoreduction to CH_4

L. Collado[a], A. Reynal[b], J.M. Coronado[a], D.P. Serrano[a,c], J.R. Durrant[b], V.A. de la Peña O'Shea[a,*]

[a] Thermochemical Process Unit, IMDEA Energy Institute, Technology Park of Móstoles, Avenida Ramón de la Sagra, 28935 Móstoles, Madrid, Spain
[b] Department of Chemistry, Imperial College London, Exhibition Road, London SW7 2AZ, United Kingdom
[c] Department of Chemical and Energy Technology, ESCET, Rey Juan Carlos University, c/Tulipán s/n, 28933 Móstoles, Madrid, Spain

ARTICLE INFO

Article history:
Received 15 July 2014
Received in revised form
10 September 2014
Accepted 15 September 2014
Available online 22 September 2014

Keywords:
Surface plasmon
Gold nanoparticles
CO_2 photoreduction

ABSTRACT

Various gold-supported TiO_2 catalysts (0.5–3.0 wt.%) were prepared by a deposition–precipitation method, and their photocatalytic activity towards CO_2 reduction was tested in the gas phase while using H_2O as electron donor and UV and visible light as energy sources. CO and H_2 are detected as major products in bare TiO_2. However, the deposition of small Au nanoparticles (NPs) onto TiO_2 was found to quantitatively enhance the reduction of CO_2 mainly to methane and C_{2+} hydrocarbons. Transient absorption spectroscopy was used to correlate the improved CH_4 production with an increased charge separation due to the electron transfer between the TiO_2 and Au NPs. The amount of Au loaded onto TiO_2 was optimized, with 1.0 wt.% showing the highest photocatalytic activity under UV light. Under visible irradiation, H_2 and CH_4 were identified as the main products, although showing significantly lower productions.

1. Introduction

The conversion of CO_2 into fuels is nowadays considered as a very promising research field to reduce the consumption of fossil fuels and the emission of greenhouse gases [1]. CO_2 is an abundant feedstock and has a wide range of industrial applications (e.g. propellant, monomer feedstock, chemical production, etc.). Nevertheless, only less than 1% of the global anthropogenic CO_2 is employed for these purposes, and the rest is released to the atmosphere due to the lack of demand or affordable conversion technologies [2,3]. One of the biggest obstacles for the development of these processes resides in the large energy input required for its transformation, which is thermodynamically unfavourable [4–6]. However, the environmental and economical advantages of converting CO_2 into valuable compounds (fuels and chemicals), has fostered an active research on the development of innovative processes for the utilization of CO_2 as chemical feedstock (including thermal reforming, plasma reforming and the photo- or photoelectro reduction) [3]. Amongst them, the photocatalytic conversion of CO_2 and water vapour, i.e. artificial photosynthesis, is a promising route for the production of light organic compounds and fuels under relatively mild conditions [7–9]. In 1970s, pioneering research of Fujishima and co-workers [10,11] reported not only the photo-assisted water splitting but also the CO_2 reduction using different semiconductor materials. Since this initial report, a large number of publications have been focused on the improvement of the photocatalytic efficiencies and the understanding of the reaction mechanism. The photoreduction of CO_2 is a complex multi-electron process that becomes even more challenging when using water as electron donor. Generally, one of the major difficulties of CO_2 reduction is the control of the product selectivity, due to the large variety of products usually obtained (including CO, CH_4 and C2–C4 hydrocarbons as well as various oxygenates, such as CH_3OH, CH_2OH or CHOOH). A second difficulty arises from the use of water as electron source, when the high competitive H_2O reduction to form H_2 is more favourable than the CO_2 reduction [4,12,13]. Up to now, TiO_2 has been the most explored semiconductor for photocatalytic applications due to its outstanding chemical and thermal stability [14]. Nevertheless, one of the main drawbacks of this photocatalyst is its fast electron/hole recombination rates, typically taking place in the microsecond to millisecond timescale [15–17]. Therefore, in order to achieve the production of valuable chemicals, it is necessary to increase the lifetime of the charge-separated state to the timescale in which the catalytic CO_2 reduction takes place. In this regard, a widely successful strategy consists in the modification of semiconductor materials with suitable metal nanoparticles

* Corresponding author. Tel.: +34 91 737 11 41.
E-mail address: victor.delapenya@imdea.org (V.A. de la Peña O'Shea).

http://dx.doi.org/10.1016/j.apcatb.2014.09.032
0926-3373/

that can store the electrons photogenerated in the semiconductor, as well as can act as co-catalysts facilitating the CO_2 activation [18–20]. In addition, the deposition of noble metal nanoparticles (NPs) having surface plasmon resonance effect (SPR), such as Au or Ag, has been demonstrated as an effective way to expand the photoresponse of the catalyst towards the visible region, reduce the fast recombination of the photogenerated charge carriers and therefore, enhance its photocatalytic activity [21–32]. In particular, photosensitization of TiO_2 with Au NPs is particularly interesting due to the low loadings generally needed to achieve the highest photocatalytic activities (typically below 1.0 wt.%) [23].

In this work, we report the effect of Au NPs supported with different loadings onto TiO_2 for the gas phase photocatalytic CO_2 reduction with water as electron donor for hydrocarbon production. The experiments were performed using two different irradiation sources (UV and visible light). The higher photocatalytic activities observed for Au/TiO_2 samples compared to the bare semiconductor are correlated with the more efficient and longer-lived charge separation measured by transient absorption spectroscopy.

2. Experimental

2.1. Synthesis of Au/TiO_2 catalysts

Commercial anatase-type titanium dioxide (TiO_2, PC500) was supplied by CrystalACTIV^{TM}. Prior to use, TiO_2 was stabilized with a thermal treatment at 400 °C for 4 h. Au/TiO_2 catalysts containing different gold percentages were prepared by a deposition–precipitation method, initially developed by Haruta and co-workers [33]. In this procedure, a solution of $HAuCl_4{\cdot}3H_2O$ (Strem Chemicals) was used as precursor. Four aqueous solutions were prepared, containing 0.5, 1.0, 1.5 and 3.0 wt.% of Au in 300 mL of Milli-Q water. The solutions were adjusted to pH 9 by addition of a 0.1 M solution of NaOH. Once the pH value was stable, 200 mg of TiO_2 were added under vigorous stirring. The deposition–precipitation procedure was done at 70 °C, maintaining the pH constant during 2 h, and then the slurry was stirred overnight. The catalysts were recovered, filtered, washed with Milli-Q water and dried at 100 °C overnight. Finally, Au/TiO_2 catalysts were calcined in air at 200 °C during 4 h using a ramp of temperatures with a rate of 5 °C/min. Samples were labelled as xAu/TiO_2, where x indicates the nominal gold loading (0.5–3.0 wt.%).

For spectroscopic measurements, analogous nanocrystalline Au/TiO_2 films were employed. Firstly, anatase TiO_2 films were prepared from a colloidal paste by the Doctor Blade technique as reported previously [34]. The films were dried for 10 min before being calcined in air at 450 °C during 30 min, and cut in small pieces of approximately 1 cm × 1.5 cm. The thickness of the films was found to be 4 μm by profilometry (Tencor Instruments). Au/TiO_2 films were prepared by coating Au nanoparticles over the TiO_2 films by photodeposition of an aqueous $HAuCl_4{\cdot}xH_2O$ solution (0.1 M), when irradiating the nanoparticulate suspension with a xenon lamp (75 W) during 5 s. To ensure that all Au^{3+} was reduced to Au, the films were irradiated for 1 h under a N_2 atmosphere with a Nd-YAG laser with a wavelength of 355 nm (350 μJ/cm^2, 10 Hz).

2.2. Characterization of prepared catalysts

Crystal structures of Au/TiO_2 samples were characterized by using a X-ray diffractometer (Philips PW 3040/00 X'Pert MPD/MRD) with Cu Kα radiation (k = 1.54178 Å) at a scanning rate of 0.2° s^{-1}. Specific surface areas were calculated from N_2 adsorption–desorption isotherms at 77 K measured on a QUADRASORB instrument. The sample was degassed at 105 °C for 20 h in N_2 before the measurement. The pore size distribution of mesopores in the samples was analyzed by BJH method. The gold content was measured by ICP-OES analyses with a Perkin Elmer Optima 3300 DV instrument by digesting the solid in a mixture of HF and HNO_3. The morphology of particles was observed by using a Philips Technai 20 Transmission Electron Microscope, operating with a tungsten filament working at 200 kV. Ultraviolet–visible diffuse reflectance spectra (UV–Vis DRS) of powdered samples were obtained by a Perkin Elmer Lambda 1050 UV/Vis/NIR spectrometer. Photoluminescence experiments were carried out with a Fluorescence Spectrometer Perkin Elmer LS 55, using an excitation wavelength of 300 nm and a cut-off filter at 350 nm.

The microsecond-second transient absorption decays were recorded using an experimental set up described previously [15]. The third harmonic of an Nd:YAG laser (355 nm), at a frequency of 1 Hz and an intensity of 350 μJ/cm^2, was used as excitation source. The kinetics of charge separation were studied by monitoring the photogenerated charge carriers in the TiO_2, with no signals from the Au nanoparticles being apparent in the spectral range studied (460–900 nm). The decays corresponding to photogenerated holes in TiO_2 were monitored at 460 nm, and electrons at 900 nm. The decays observed are the average of 500 laser pulses.

2.3. Photocatalytic CO_2 reduction tests

CO_2 photoreduction experiments were conducted in a home-made reaction system in continuous-flow mode. The gas-phase photoreactor, with an effective volume of 280 mL, was made of steel and provided with a borosilicate window for irradiation. The powdered catalyst (0.1 g) was deposited on a glass microfiber filter and fitted inside the reactor. UV illumination was carried out using four 6 W lamps with a maximum wavelength at 365 nm and an average intensity of 71.7 W m^{-2} (measured by a Blue-Wave spectrometer in the range 330–400 nm), while a 30 W white light LED with cut-off filters at 400 nm and 455 nm was used for visible light illumination. Pure CO_2 (99.9999%, Praxair) and water (Milli-Q), were passed through a Controller Evaporator Mixer (CEM) maintaining a molar ratio of 7.25 (CO_2:H_2O) to generate a reaction feed of CO_2 and water vapour. The reaction conditions were set at 2 bars and 50 °C. Continuous gas chromatography analyses were performed to detect the reaction products. GC (Bruker 450-GC) was equipped with two separation branches and two sampling loops. The first separation branch was equipped with two semicapillary columns (BR-Q Plot and BR-Molesieve 5A). This branch was also equipped with a Thermal Conductivity Detector (TCD), a Flame Ionization Detector (FID) and a methanizer. The second separation branch consisted on a capillary column (CP-Sil 5B) and a second Flame Ionization Detector (FID).

Before starting the experiments, the catalysts were first pretreated using the following method: the reactor was firstly degassed at 80 °C under vacuum and then purged with Ar (100 mL/min) for 1 h in order to remove any residual organic compounds weakly adsorbed to the surface of the catalyst. Then, the reactor was flushed with the CO_2 and H_2O mixture for 1 h to establish an adsorption–desorption balance at the reaction temperature. Prior to illumination, the reactor was pressurized with the mixture and kept at a reduced flow rate for another 1 h.

No products were found after performing blank experiments under dark conditions or without any catalyst under UV or visible illumination. Further, experiments with high purity Ar (99.999%, Praxair) were also performed to control the carbon contamination on the surface of the catalysts. GC analyses detected small amounts of CO_2 (ca. less than 200 ppm from air) in the feed composition before starting the illumination, indicating a small carbon contribution due to impurities of the reagents, which may result in the appearance of adsorbed species such as carbonates/bicarbonates

that could participate in the photocatalytic reaction or affect its selectivity [35,36]. All photocatalytic tests were investigated over a period of 0–15 h of irradiation time and repeated at least twice to assure the accuracy of the reaction results.

The Formal Quantum Efficiency (FQE) was calculated using Eq. (1), considering the incident light intensity in the wavelength range of 325–400 nm:

$$\text{FQE} = \frac{\text{rate of reaction (molecules/s)}}{\text{incident light intensity (photons/s)}} \quad (1)$$

3. Results and discussion

3.1. Characterization

To determine the effect of Au nanoparticles to the physicochemical properties and the photocatalytic behaviour of TiO_2, four samples with different Au nominal loadings (0.5, 1.0, 1.5 and 3.0 wt.%) were prepared by a deposition–precipitation method. The metal content, determined by ICP analysis (Table 1), indicates that the total nominal gold content present in the synthesis solution is not completely deposited on the surface of the semiconductor. This behaviour was previously observed by Haruta's group [33] and was mainly attributed to the high pH value of the solution (i.e. pH 9), which compared to the point of zero charge of the TiO_2 ($PZC_{TiO_2} \sim 6$), limits the number of adsorption sites and restricts the gold content. These studies also show that the efficiency of the metal deposition diminishes as increasing the Au content.

The structural properties of the photocatalysts were evaluated by X-ray diffraction (Fig. 1) and all profiles can be indexed to the TiO_2 anatase phase (ICDD No. 21-1272, space group: I41/amd). For metal loaded TiO_2 samples, no reflection peaks from Au are observed due to the low concentration or the small crystallite size of Au NPs. The average crystal sizes of TiO_2 were estimated, before and after Au deposition, using the Scherrer's equation on the anatase (1 0 1) diffraction peak at ca. $2\theta = 25.3^\circ$ (Table 1). All the samples have almost the same crystallite size, indicating that the deposition of Au did not evidently

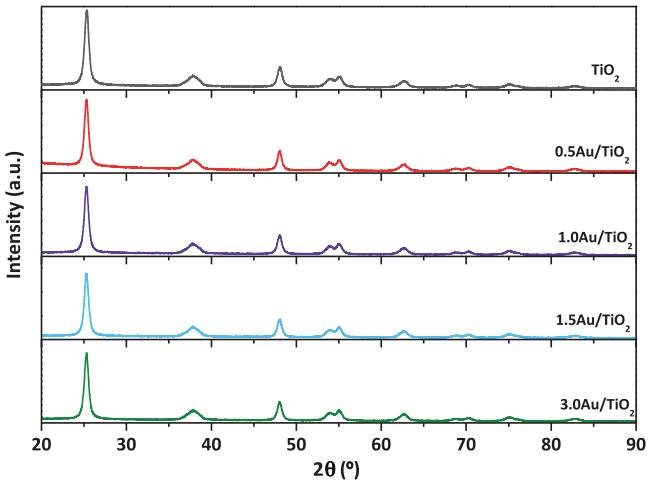

Fig. 1. XRD patterns of TiO_2 and Au/TiO_2 samples.

alter the crystalline phase or structural properties of TiO_2. In addition, the morphology of TiO_2 as well as the presence and size of Au NPs is studied by TEM imaging (Fig. 2). Commercial anatase exhibits nanosized particles (10–15 nm) with small and well dispersed Au NPs of diameter ranging between 1.9 and 3.0 nm. Gold particle size enlarged when increasing the gold content.

The textural properties of the catalysts were analyzed by N_2 adsorption–desorption isotherms (Fig. 3). All samples exhibit type II isotherms with a hysteresis loop (type H3) at relative high pressure (ca. $p/p_0 > 0.4$), which indicates the presence of meso- and macropores usually originated from the agglomeration of primary crystallites [37]. Table 1 summarizes the quantitative data of BET surface area, pore volume and average pore size in order to detect variations between samples before and after gold loading. After the deposition of Au NPs onto TiO_2, the surface area and pore volume decreased due to a partial blocking of TiO_2 pores by Au NPs,

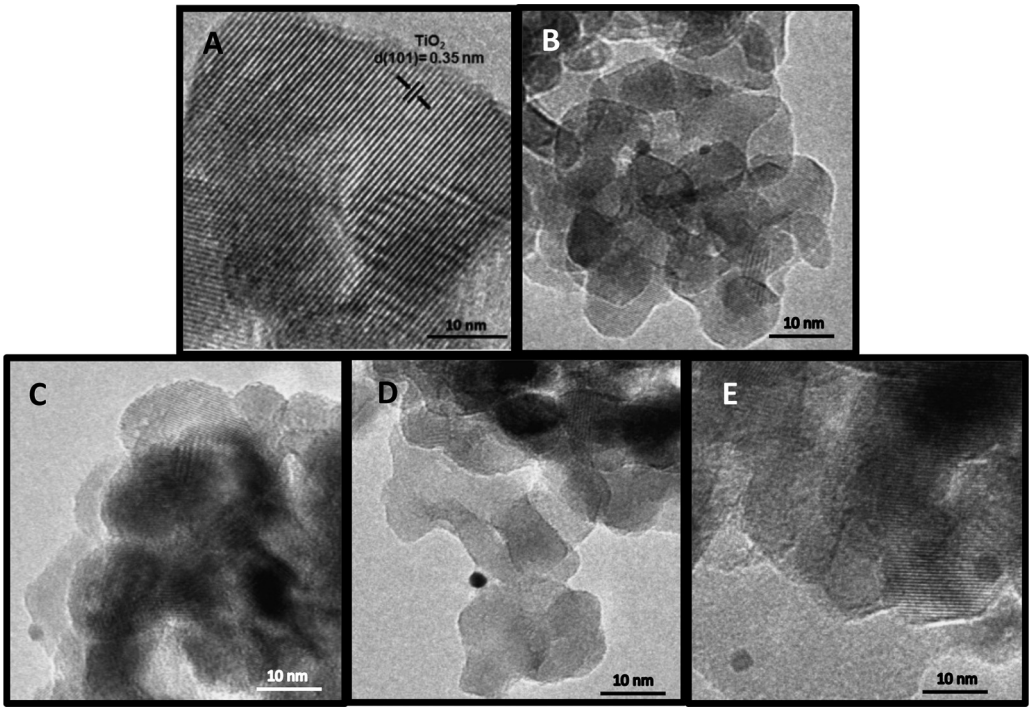

Fig. 2. TEM micrographs of TiO_2 (A); $0.5Au/TiO_2$ (B); $1.0Au/TiO_2$ (C); $1.5Au/TiO_2$ (D); $3.0Au/TiO_2$ (E).

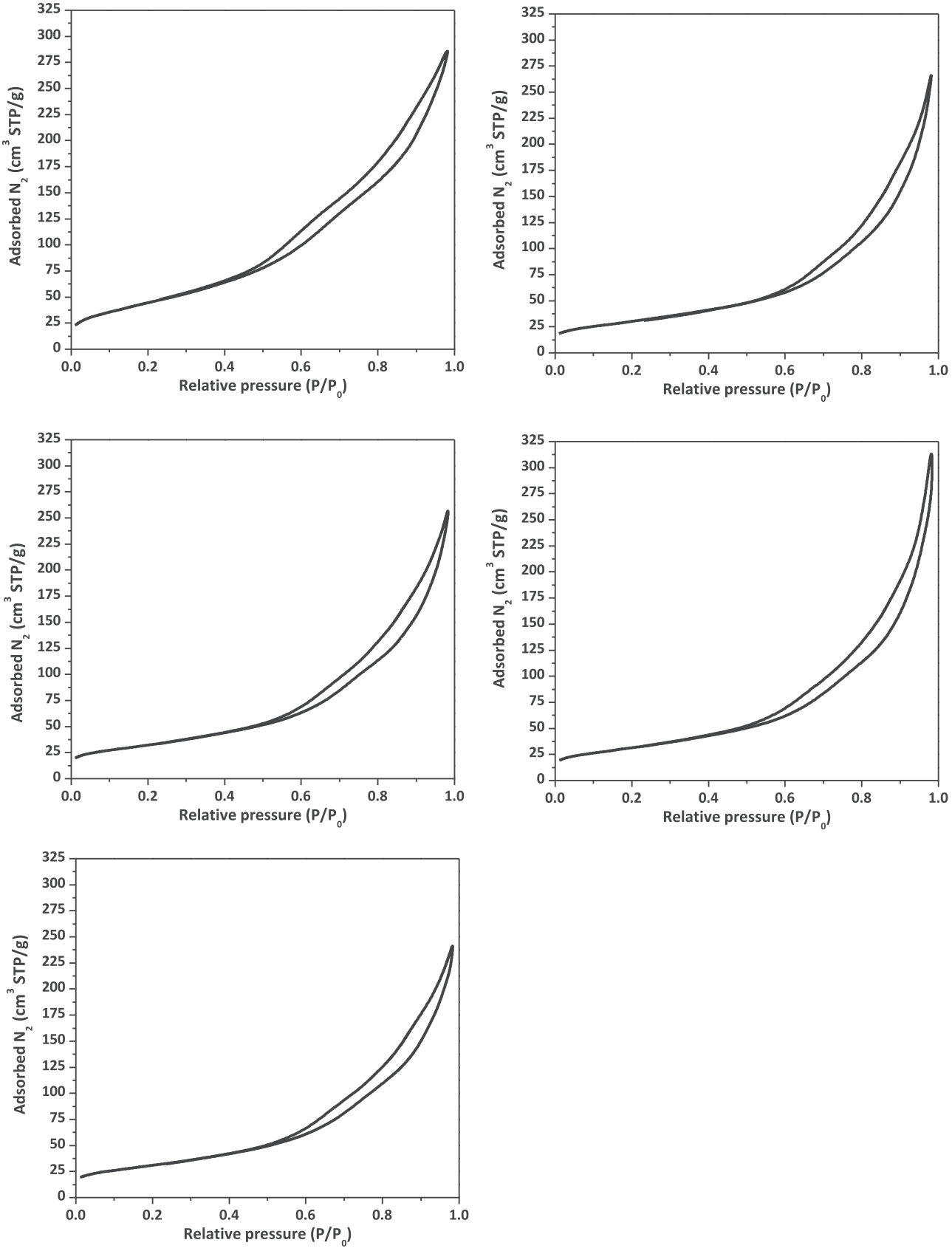

Fig. 3. N_2 adsorption/desorption isotherms of TiO_2 and Au/TiO_2 samples.

Table 1
Physicochemical properties of bare TiO_2 and Au/TiO_2 catalysts (0.5–3.0 wt.% Au).

Sample	Nominal Au (wt.%)	Experimental Au (wt.%)[a]	Crystal size (nm)[b]	S_{BET} (m^2/g)	Pore volume ($cm^3\ g^{-1}$)	Pore size (nm)	D_{Au} (nm)[c]
TiO_2	–	–	14.5	165.8	0.44	4.7	–
$0.5Au/TiO_2$	0.5	0.29	15.8	122.7	0.41	5.6	1.9
$1.0Au/TiO_2$	1.0	0.42	15.9	116.2	0.40	5.6	2.1
$1.5Au/TiO_2$	1.5	0.56	14.5	112.8	0.39	5.7	2.9
$3.0Au/TiO_2$	3.0	0.96	14.8	111.1	0.38	5.7	3.1

[a] Au content (wt.%) measured by ICP-OES.
[b] Crystal size calculated by XRD.
[c] Au particle size determined by TEM.

which was more noticeable when increasing the gold content [38]. In addition, the possible appearance of hot spots in the metal NPs surroundings during the second calcination treatment, may cause the sintering of TiO_2 nanoparticles, and consequently contribute to the decrease in the surface area and in the pore volume.

The diffuse reflectance spectra (DRS) of the bare TiO_2 and Au/TiO_2 catalysts are shown in Fig. 4A. The broad absorption band observed at wavelengths shorter than 400 nm is attributed to the excitation of electrons from the valence band to the conduction band of TiO_2. For all samples, the band gap values (E_g = 3.3 eV) almost remained unchanged even after Au loading. In addition, Au/TiO_2 samples exhibit significantly enhanced light absorption in the visible region showing a broad band located between 450 and 600 nm, typical of the SPR of Au NPs. The lower intensity of this band in $0.5Au/TiO_2$ catalyst is correlated to its minor gold content.

Fig. 4B depicts the photoluminescence (PL) spectra of TiO_2 anatase and Au/TiO_2 catalysts in the wavelength range of 300–650 nm. A broad band from 350 to 600 nm (3.5–2.1 eV) composed by multiple emission contributions is observed for all catalysts. The UV emission peak located at 396 nm is attributed to the band to band radiative recombination process with the energy of light close to the band gap energy of anatase (E_g = 3.2 eV; 387 nm) [37,39]. PL bands appearing in the visible region (400–600 nm) are mostly associated with excitons, which mainly result from surface oxygen vacancies and defects [39–42]. Fig. 4B shows a significantly smaller band to band PL amplitude for Au/TiO_2 compared to TiO_2 catalysts, suggesting a decrease in the rate of electron/hole recombination when the semiconductor is functionalized with Au NPs [22]. The quenching of the luminescence of Au/TiO_2 samples increases with the loading of Au NPs, reaching a saturation point when the amount of Au is greater than 1 wt.%. This behaviour is

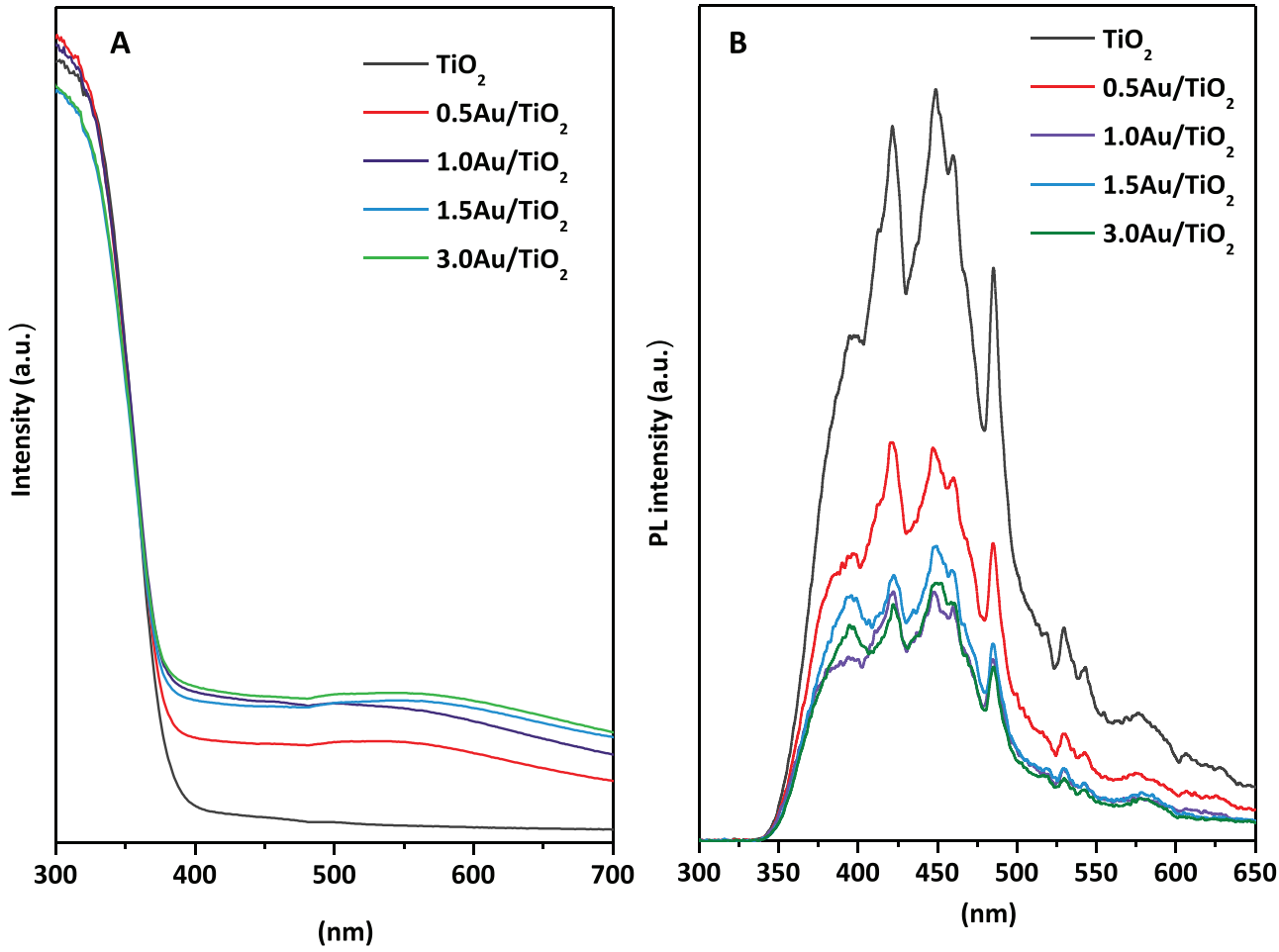

Fig. 4. Diffuse reflectance UV–vis (A) and emission spectra of TiO_2 and Au/TiO_2 (B) photocatalysts.

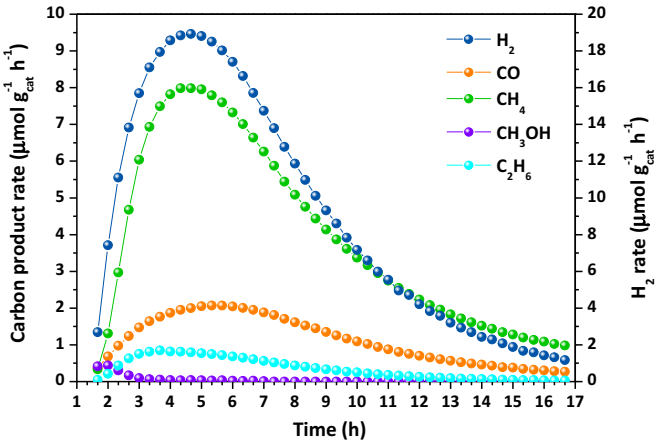

Fig. 5. Temporal evolution of the photoreduction products using a 0.5Au/TiO_2 photocatalyst under UV irradiation.

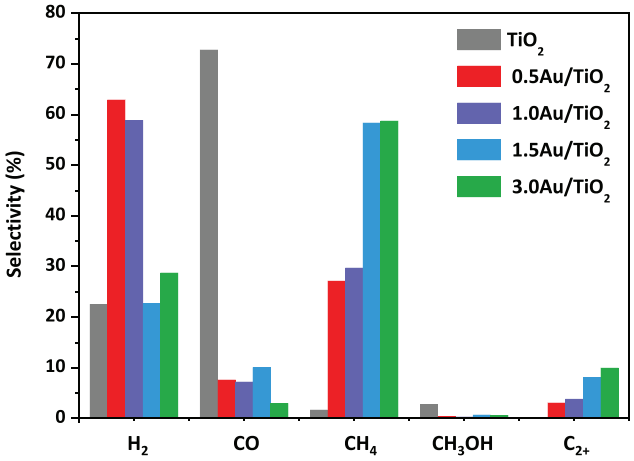

Fig. 6. Product selectivity over TiO_2 and Au/TiO_2 photocatalysts (0.5–3.0 wt.% Au) after 15 h of UV irradiation.

in good agreement with the absorption intensities corresponding to the SPR, which shows smaller signal amplitude for 0.5Au/TiO_2 (Fig. 4A).

3.2. Photocatalytic CO_2 reduction

The effect of Au NPs to the CO_2 photoreduction activity of Au/TiO_2 catalysts was investigated under UV and visible light illumination. Variations in the product distribution were studied for TiO_2 loaded with different metal contents (0.5–3 wt.% Au). Previous CO_2 photoreduction studies performed with anatase-type TiO_2 showed high selectivities towards the formation of CO and H_2 for the bare semiconductor [22]. We show herein that, the deposition of Au metal nanoparticles onto TiO_2 results in an improved hydrocarbon formation (high electron demanding products) mainly attributed to the enhanced charge separation and improved multielectron transfer processes.

Fig. 5 shows the kinetics of the product distribution of 0.5Au/TiO_2 catalyst under UV irradiation. The two main reaction products detected were H_2 and CH_4, which evolved at a similar trend reaching the maximum reaction rate after 4 h of UV irradiation (18.9 μmol g_{cat}^{-1} h^{-1} and 8.0 μmol g_{cat}^{-1} h^{-1} for H_2 and CH_4, respectively). CO, CH_3OH and C_2H_6 were also observed, although showing much lower reaction rates.

In order to further investigate the influence of Au loading to the efficiency of CO_2 photoreduction, the selectivity of the photogenerated products by bare TiO_2 and Au/TiO_2 catalysts is compared (Fig. 6). In agreement with previous observations, CO, H_2 and minor amounts of CH_3OH were produced with bare TiO_2. On the contrary, the selectivity of Au/TiO_2 samples completely shifted towards the production of C1 and C2 hydrocarbons, being CH_4 the main component, due to the aforementioned improved electron transfer processes. This better charge separation influences also a higher selectivity to H_2 due to an increased water decomposition rate. This behaviour also agrees with the enhanced hydrocarbon formation (high electron demanded products) and the decrease in the CO evolution, which was almost 10 times lower with respect to that of TiO_2.

The effect of the metal loading to the CO_2 reduction photocatalytic activity is evaluated by comparing the kinetics and accumulated production of CH_4 (Fig. 7). The kinetic profiles of all samples show a similar trend, with productions reaching maximum values after 4–6 h of irradiation (Fig. 7A). Prolonged exposure of the catalysts to light led to a progress decrease in the reaction rates for all products. The highest CH_4 production was obtained with 1.0Au/TiO_2 sample at a maximum rate of ca. 8.86 μmol g_{cat}^{-1} h^{-1} reached before 5 h of illumination. Lower and higher Au contents lead to a decrease in the CO_2 reduction kinetic profiles, being the lowest rate for 3.0Au/TiO_2 sample. In addition, it can be observed that an increase of the metal loading leads to a larger deactivation. Fig. 7B represents a comparison of the cumulative production of CH_4 over selected Au catalyst and bare TiO_2 semiconductor, also including formal quantum efficiency (FQE) values. In this case, the deposition of Au NPs results in a quantitatively improved CH_4 formation, which is more than 12 times higher than that obtained with bare TiO_2. The highest CH_4 production at 15 h is obtained with 1.0Au/TiO_2 photocatalyst (74.1 μmol g_{cat}^{-1} and a FQE of 0.068).

The enhanced CH_4 production of Au/TiO_2 photocatalysts can be explained from different approaches. From the optoelectronic point of view, the decrease in the emission intensity of Au/TiO_2 samples observed in the PL studies (Fig. 4B) was ascribed to a possible decrease in the e^-/h^+ recombination rate that favours the CO_2 photoreduction. To confirm this hypothesis we studied the kinetics of charge separation and charge recombination in TiO_2 and Au/TiO_2 catalysts by transient absorption spectroscopy (TAS) (Fig. 8A). The signal corresponding to photoexcited holes in the TiO_2 is monitored at 460 nm, while electrons are probed at 900 nm. The decays of photogenerated electrons and holes in bare TiO_2 show identical kinetics with $t_{50\%}$~50 μs due to bimolecular recombination [15,43]. The deposition of Au NPs onto TiO_2 affects both the dynamics of photogenerated electrons and holes: On one hand, the transient absorption signal corresponding to photoexcited electrons in TiO_2 shows a smaller amplitude for Au/TiO_2 films when compared to that of bare TiO_2 (Fig. 8B). This observation is indicative of a fast (<10 μs) electron transfer from the semiconductor to the Au NPs. Secondly, the transient absorption signal amplitude assigned to photoexcited holes when the TiO_2 is loaded with Au NPs exhibits a 3-fold increase when compared to that of bare TiO_2. This increase in the signal amplitude is assigned to the accumulation of holes in the TiO_2 after the fast electron transfer from the semiconductor to the metal nanoparticles.

The decay dynamics of the charge carriers can provide an indication of the lifetime of the charge separated state. While the transient absorption decay of photoholes in bare TiO_2 exhibit a $t_{50\%}$~50 μs due to bimolecular electron/hole recombination, the lifetime of the holes accumulated at the TiO_2 valence band in Au/TiO_2 catalysts is $t_{50\%}$~350 μs. Thus, our results indicate that the deposition of Au NPs on TiO_2 results in a 7-fold increased lifetime of the charge separated state when compared to bare TiO_2. Our results demonstrate that Au NPs can efficiently store the electrons photogenerated in the

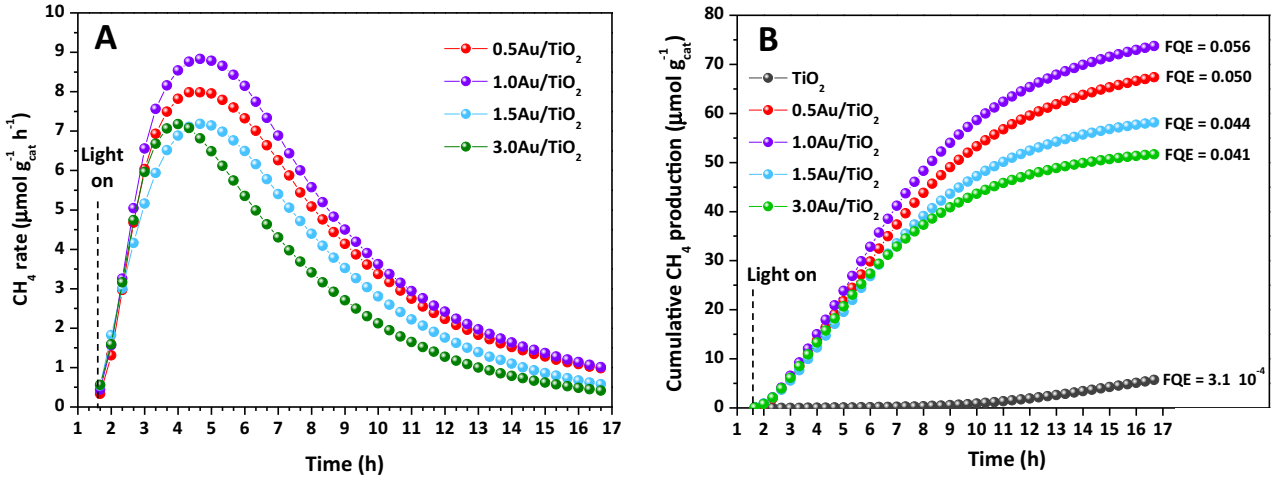

Fig. 7. Effect of the gold loading on the CH_4 production in terms of evolution rates (A) and cumulative production (B) under UV irradiation.

semiconductor, which become readily available to drive the multi-electron CO_2 reduction process. Fig. 8C schematizes this enhanced UV-light driven mechanism observed in Au/TiO_2 catalysts. Here, the presence of Au NPs, in direct contact with TiO_2 favours the transfer of photogenerated electrons from the semiconductor to the metal. This charge transfer and the subsequent accumulation of electrons in the Au NPs involve the equilibration of the apparent Fermi level in the Au/TiO_2 composite [44,45]. This level is expected to shift to more negative potentials in small Au NPs, thus leading to more reductive catalysts [46].

On the other hand, the different photocatalytic performance due to the Au loading can be explained from the structural point of view. The highest yields are obtained with low loaded Au/TiO_2 catalysts which exhibit the smallest Au NPs size (Table 1). This behaviour agrees with the studies performed by Kamat et al. They reported the size-dependency of Au NPs in the

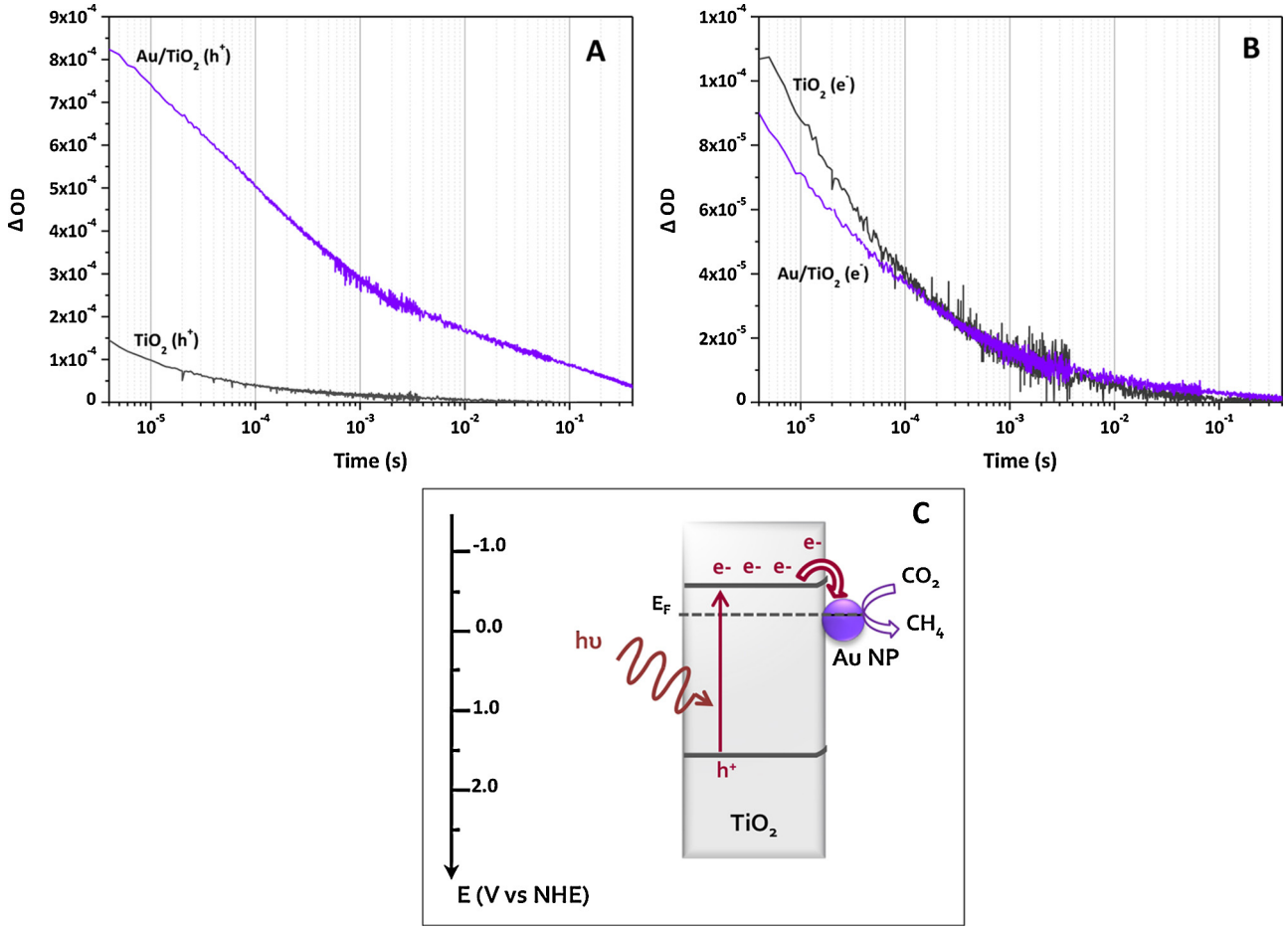

Fig. 8. Transient absorption decays of holes (A) and photogenerated electrons (B) in TiO_2 and Au/TiO_2 after excitation at 355 nm, and schematic of the reaction mechanism for UV-light driven CO_2 photoreduction over Au/TiO_2 catalysts, showing the equilibrated Fermi level of TiO_2 once Au NPs are in contact with the semiconductor (C).

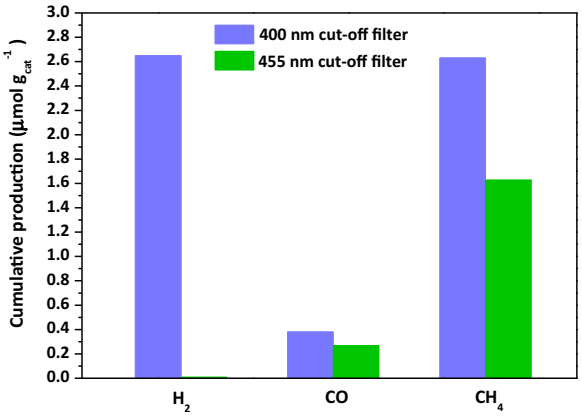

Fig. 9. Comparison of the cumulative production for 1.0Au/TiO_2 catalyst after 15 h of visible light irradiation, using a LED lamp with 400 and 455 nm cut-off filters.

photocatalytic performance, demonstrating that catalysts with small metal NPs are more active than those composed of larger particles due to the more reductive character of the composite [46]. Based on the observations stated above, 1.0Au/TiO_2 was selected as the catalyst with the optimum metal content in our experimental conditions.

The activity of 1.0Au/TiO_2 towards CO_2 photoreduction was also evaluated under visible light irradiation (Fig. 9). Under wavelengths above 400 nm, the gold photocatalyst was active towards CO, CH_4 and H_2 formation, although the productions were significantly lower than under UV irradiation. Since TiO_2 light absorption is below to 400 nm, different models have been reported in the literature to explain the photoactivity under visible irradiation. On one hand, this behaviour is attributed to the excitation of sub-band gap electrons from surface defects. In the case of Au/TiO_2 photocatalysts the formation of these electron/hole pairs near the surface of the TiO_2 is promoted due to the strong electric field created by the surface plasmons of Au NPs [27,47,48]. Additionally, other studies have reported photoactivities mediated by a direct transfer of excited electrons from Au NPs to the conduction band (CB) of TiO_2 [27,49,50]. This electron injection, only allowed across an energy barrier of 1.0 eV [51–54], can be achieved by the excitation of electrons in the filled d-band of gold to electronic states above the Fermi level (E_F) [50,48].

In order to clarify the photoelectron transfer behaviour additional photocatalytic experiments were performed using a 455 nm cut-off filter. As shown in Fig. 9, 1.0Au/TiO_2 still shows photoactivity towards CH_4 and CO, suggesting that gold NPs participate in the visible light induced performance. The decreasing in H_2 formation under these conditions might suggest that hydrogen evolution proceeds via the excitation of sub-band gap states of TiO_2, rather from the direct excitation of Au NPs. Further experiments are necessary to elucidate the specific mechanism of the enhanced photocatalytic activity facilitated by the SPR of Au NPs.

4. Conclusions

The results shown herein demonstrate that the functionalization of TiO_2 with Au nanoparticles is effective at increasing the lifetime of charge separated states through interfacial electron transfer. Under UV irradiation, Au/TiO_2 catalysts are found to be more active than bare TiO_2 for the production of high electron-demanding products. Low loadings of Au onto the TiO_2 resulted in an enhancement of the hydrocarbon production, especially CH_4. This behaviour is explained in terms of a decrease of the charge recombination rates due to the electron scavenging ability of Au NPs. The physical separation of charge carriers results in a 7-fold longer lived state compared to bare TiO_2 films, which is crucial in order to perform the slow and multi-electron demanding CO_2 reduction reaction.

On the other hand, Au/TiO_2 catalysts show photoactivity towards the visible light driven CO_2 photoreduction, although yields are significantly lower than under UV irradiation. This slight photoactivity is attributed to two possible mechanisms: the weak sub-band gap absorption created due to the presence of impurity states located below the TiO_2 conduction band, and on the other hand, the interaction of the strong electric field created by the surface plasmons of Au NPs with TiO_2. This effect may allow the formation of electron/hole pairs in the near surface region of TiO_2, enhancing the CH_4 yields.

Acknowledgments

Financial support from the Spanish Ministry of Economy and Competitiveness (project ENE2009-09432) and the ERC (project Intersolar 291482, to J.D.) is gratefully acknowledged. V.A.P.O. and L.C. thank funding provided by the grants Ramón y Cajal (RYC-2008-02069) and FPI (BES-2010-032400), respectively. A.R. thanks the European Commission Marie Curie (PCIG10-GA-2011-303650).

References

[1] M. Aresta, A. Dibenedetto, A. Angelini, Chem. Rev. 114 (2014) 1709.
[2] B. Hu, C. Guild, S.L. Suib, J. CO_2 Util. 1 (2013) 18.
[3] M. Tahir, N.S. Amin, Renew. Sustain. Energy Rev. 25 (2013) 560.
[4] J. Hong, W. Zhang, J. Ren, R. Xu, Anal. Methods 5 (2013) 1086.
[5] K. Li, D. Martin, J. Tang, Chin. J. Catal. 32 (2011) 879.
[6] V.A. De La Peña O'Shea, J.M. Coronado, D.P. Serrano, Dyna 87 (2012) 145.
[7] R.K. De_Richter, T. Ming, S. Caillol, Renew. Sustain. Energy Rev. 19 (2013) 82.
[8] A. Bazzo, A. Urakawa, ChemSusChem 6 (2013) 2095.
[9] W.-H. Lee, C.-H. Liao, M.-F. Tsai, C.-W. Huang, J.C.S. Wu, Appl. Catal. B: Environ. 132–133 (2013) 445.
[10] A. Fujishima, K. Honda, Nature 238 (1972) 37.
[11] K.H.T. Inoue, A. Fujishima, S. Konishi, Nature 277 (1979) 637.
[12] A.D. Handoko, K. Li, J. Tang, Curr. Opin. Chem. Eng. 2 (2013) 200.
[13] M. Mikkelsen, M. Jørgensen, F.C. Krebs, Energy Environ. Sci. 3 (2010) 43.
[14] P.D. Tran, L.H. Wong, J. Barber, J.S.C. Loo, Energy Environ. Sci. 5 (2012) 5902.
[15] A. Reynal, F. Lakadamyali, M.A. Gross, E. Reisner, J.R. Durrant, Energy Environ. Sci. 6 (2013) 3291.
[16] J. Tang, J.R. Durrant, D.R. Klug, J. Am. Chem. Soc. 130 (2008) 13885.
[17] A. Yamakata, T. Ishibashi, H. Onishi, J. Phys. Chem. B 105 (2001) 7258.
[18] S. Neaţu, J.A. Maciá-Agulló, H. Garcia, Int. J. Mol. Sci. 15 (2014) 5246.
[19] V.A. de la Peña O'Shea, S. González, F. Illas, J.L.G. Fierro, Chem. Phys. Lett. 454 (2008) 262.
[20] J.M. Coronado, F. Fresno, M.D. Hernández-Alonso, R. Portela, Design of Advanced Photocatalytic Materials for Energy and Environmental Applications, Springer, 2013 (Chapter 10).
[21] V.K. Prashant, J. Phys. Chem. Lett. 3 (2012) 663.
[22] L. Collado, P. Jana, B. Sierra, J.M. Coronado, P. Pizarro, D.P. Serrano, V.A. de la Peña O'Shea, Chem. Eng. J. 224 (2013) 128.
[23] A. Corma, H. Garcia, J. Catal. 308 (2013) 168.
[24] S.G. Kumar, L.G. Devi, J. Phys. Chem. A 115 (2011) 13211.
[25] Z. Zhang, J.T. Yates, Chem. Rev. 112 (2012) 5520.
[26] E. Grabowska, A. Zaleska, S. Sorgues, M. Kunst, A. Etcheberry, C. Colbeau-Justin, H. Remita, J. Phys. Chem. C 117 (2013) 1955.
[27] D. Jose, C.M. Sorensen, S.S. Rayalu, K.M. Shrestha, K.J. Klabunde, Int. J. Photoenergy 2013 (2013) 1.
[28] H. Li, W. Lu, J. Tian, Y. Luo, A.M. Asiri, A.O. Al-Youbi, X. Sun, Chem. Eur. J. 18 (2012) 8508.
[29] C.-T. Dinh, H. Yen, F. Kleitz, T.-O. Do, Angew. Chem. Int. Ed. Engl. (2014) 1.
[30] Y. Lu, H. Yu, S. Chen, X. Quan, H. Zhao, Environ. Sci. Technol. 46 (2012) 1724.
[31] W. Hou, Z. Liu, P. Pavaskar, W.H. Hung, S.B. Cronin, J. Catal. 277 (2011) 149.
[32] E. Kowalska, O. Omar, P. Mahaney, Phys. Chem. Chem. Phys. 12 (2010) 2344.
[33] M. Haruta, T. Kobayashi, H. Sano, N. Yamada, Chem. Lett. (1987) 405.
[34] S. Ito, T.N. Murakami, P. Comte, P. Liska, C. Grätzel, M.K. Nazeeruddin, M. Grätzel, Thin Solid Films 516 (2008) 4613.
[35] L. Liu, Y. Li, Aerosol Air Qual. Res. 2 (2014) 453.
[36] N.M. Dimitrijevic, B.K. Vijayan, O.G. Poluektov, T. Rajh, K.A. Gray, H. He, P. Zapol, J. Am. Chem. Soc. 133 (2011) 3964.
[37] J. Yu, L. Yue, S. Liu, B. Huang, X. Zhang, J. Colloid Interface Sci. 334 (2009) 58.
[38] S. Zhu, S. Liang, Q. Gu, L. Xie, J. Wang, Z. Ding, P. Liu, Appl. Catal. B: Environ. 119–120 (2012) 146.
[39] B. Liu, L. Wen, X. Zhao, Mater. Chem. Phys. 106 (2007) 350.
[40] J. Liqiang, Q. Yichun, W. Baiqi, L. Shudan, J. Baojiang, Y. Libin, F. Wei, F. Honggang, S. Jiazhong, Sol. Energy Mater. Sol. Cells 90 (2006) 1773.

[41] L.G. Devi, B. Nagaraj, K.E. Rajashekhar, Chem. Eng. J. 181–182 (2012) 259.
[42] B. Choudhury, M. Dey, A. Choudhury, Appl. Nanosci. 4 (2013) 499.
[43] A.J. Cowan, J. Tang, W. Leng, J.R. Durrant, D.R. Klug, J. Phys. Chem. C 114 (2010) 4208.
[44] W. Hou, S.B. Cronin, Adv. Funct. Mater. 23 (2013) 1612.
[45] H. Park, Y. Park, W. Kim, W. Choi, J. Photochem. Photobiol. C: Photochem. Rev. 15 (2013) 1.
[46] V. Subramanian, E.E. Wolf, P.V. Kamat, J. Am. Chem. Soc. 126 (2004) 4943.
[47] J. Fang, S.-W. Cao, Z. Wang, M.M. Shahjamali, S.C.J. Loo, J. Barber, C. Xue, Int. J. Hydrog. Energy 37 (2012) 17853.
[48] W. Hou, W.H. Hung, P. Pavaskar, A. Goeppert, M. Aykol, S.B. Cronin, ACS Catal. 1 (2011) 929.
[49] P.L. Jinlin Long, W.H. Jinlin Long, C. Hongjin, G. Quan, X. Jie, F. Lizhou, W. Shuchao, Z. Yangen, W. Wei, H. Ling, W. Xuxu, Energy Environ. Sci. 7 (2014) 973.
[50] J. Sá, G. Tagliabue, P. Friedli, J. Szlachetko, M.H. Rittmann-Frank, F.G. Santomauro, C.J. Milne, H. Sigg, Energy Environ. Sci. 6 (2013) 3584.
[51] A. Furube, L. Du, K. Hara, R. Katoh, M. Tachiya, J. Am. Chem. Soc. 129 (2007) 14852.
[52] J.Y. Park, H. Lee, J.R. Renzas, Y. Zhang, G.A. Somorjai, Nano Lett. 8 (2008) 2388.
[53] J. Tang, M. White, G.D. Stucky, E.W. McFarland, Electrochem. Commun. 5 (2003) 497.
[54] L. Du, A. Furube, K. Yamamoto, K. Hara, R. Katoh, M. Tachiya, J. Phys. Chem. C 113 (2009) 6454.